PeerJ Preprints NOT PEER-REVIEWED

Combined proteome and transcriptome analyses reveal that Zika virus circulating in Brazil alters cell cycle and neurogenic programmes in human neurospheres

Patricia P. Garcez[2,1@], Juliana Minardi Nascimento[1,4*], Janaina Mota de Vasconcelos[5*], Rodrigo Madeiro da Costa[1*], Rodrigo Delvecchio[3], Pablo Trindade[1], Erick Correia Loiola[1], Luiza M. Higa[3], Juliana S. Cassoli[4], Gabriela Vitória[1], Patricia Sequeira[6], Jaroslaw Sochacki[1], Renato S. Aguiar[3], Hellen Thais Fuzii[7], Ana M. Bispo de Filippis[6], João Lídio da Silva Gonçalves Vianez Júnior[5], Daniel Martins-de-Souza[4], Amilcar Tanuri[3], Stevens K. Rehen[1, 2 @]

[1]D'Or Institute for Research and Education (IDOR), Rio de Janeiro, Brazil; [2]Institute of Biomedical Sciences, Federal University of Rio de Janeiro, Rio de Janeiro, Brazil; [3] Institute of Biology, Federal University of Rio de Janeiro, Rio de Janeiro, Brazil; [4]Institute of Biology, Department of Biochemistry and Tissue Biology, University of Campinas (UNICAMP), Campinas, Brazil; [5]Center for Technological Innovation, Evandro Chagas Institute, Belém, Brazil; [6]Institute Oswaldo Cruz, FIOCRUZ, Rio de Janeiro, Brazil; [7]Federal University of Pará, Belém, Brazil

[*]Authors contributed equally to this work

[@]Corresponding authors: srehen@lance.ufrj.org and ppgarcez@gmail.com

PeerJ Preprints | https://doi.org/10.7287/peerj.preprints.2033v1 | CC-BY 4.0 Open Access | rec: 9 May 2016, publ: 9 May 2016

ZIKV infection depletes human neural progenitors and reduces neural production by upregulation of viral replication and DNA damage targets

Summary

Zika virus (ZIKV) has been associated with microcephaly and other brain abnormalities; however, the molecular and cellular consequences of Zika virus circulating in Brazil to the human brain development have not been studied yet. Here we describe alterations in human neurospheres derived from neural stem cells infected with Brazilian ZIKV. Combined proteomics and mRNA transcriptional profile analyses showed that Brazilian ZIKV, prior to induce cell death, alters cell cycle and halts neurogenic programmes, in addition to regulate transcription and protein translation due to viral replication. These results point to biological mechanisms potentially implicated in brain malformations as a result of ZIKV congenital infection.

Highlights

- ZIKV infection depletes neural progenitors and reduces neuronal production in human neurospheres
- ZIKV infection activates the DNA repair machinery and upregulates viral translation
- ZIKV infection halts cell cycle progression and neuronal differentiation genes and proteins, prior to cell death

PeerJ Preprints | https://doi.org/10.7287/peerj.preprints.2033v1 | CC-BY 4.0 Open Access | rec: 9 May 2016, publ: 9 May 2016

ETOC BLURB

Zika virus (ZIKV) has been associated with microcephaly rise in Brazil. The present study showed that ZIKV isolated in Brazil identifies more than 500 genes and proteins altered after viral infection in human neurospheres exposed to ZIKV. Prior to promote cell death, ZIKV impairs brain growth by arresting cell cycle and shutting down neurogenic programs during development of the central nervous system.

Introduction

Primary microcephaly is a rare brain malformation characterized by the reduction of cephalic perimeter. Microcephaly aetiologies vary from genetic abnormalities to external factors such as toxoplasma, rubella, cytomegalovirus, herpes virus and syphilis (TORCHS) (Gilmore and Walsh, 2013).

An increased number of cases of microcephaly associated with ZIKV has been reported in Brazil and elsewhere (Calvet et al., 2016; Mlakar et al., 2016). ZIKV is able to induce cell death in human neural progenitors (Tang et al., 2016; Garcez et al., 2016, Qian et al., 2016) and to impair the growth of brain organoids (Garcez et al., 2016, Qian et al., 2016). Still, the molecular fingerprint of neural stem cells infected with ZIKV has not been thoroughly investigated yet.

Here we examine the transcriptome and proteome of human neurospheres derived from neural stem cells exposed to ZIKV isolated in Brazil. We show that ZIKV induces responses to DNA damage, cell cycle arrest, apoptosis and downregulation

PeerJ Preprints | https://doi.org/10.7287/peerj.preprints.2033v1 | CC-BY 4.0 Open Access | rec: 9 May 2016, publ: 9 May 2016

of neurogenic programmes. These results shed a light in a potential molecular mechanism implicated in brain malformations as a result of ZIKV congenital infection.

Results

ZIKV infects and induces cell death in human neurospheres

Sequencing of fragments of ZIKV circulating in Brazil matched the Asian ZIKV strain, confirming previous observations that ZIKV circulating in Brazil is 97-100% similar to ZIKV isolated in Asia (Calvet et al., 2016, Supplementary Fig 1A). RT-PCR discarded contamination with Dengue and Chikungunya viruses, other circulating viruses commonly found in Brazil (Supplementary Fig 1B).

Neural stem cells derived from induced pluripotent cells (iPS) cells were exposed to ZIKV (MOI 0.025) for two hours, followed by a procedure to grow neurospheres. After three days, neurospheres exposed to ZIKV became labelled with the antibody 4G2 against flavivirus envelope protein, confirming the infection (Fig 1A, 1B and 1C).

To confirm that ZIKV circulating in Brazil triggers apoptosis, neurospheres were labelled with an antibody against activated caspase 3 (Fig 1D, 1E and 1F). In addition, cresyl violet staining revealed an increase in pyknotic nuclei in ZIKV-exposed neurospheres (Supplementary Fig 2A-2C). After six days *in vitro*, we observed that the number of ZIKV-exposed neurospheres was reduced by 50%

PeerJ Preprints | https://doi.org/10.7287/peerj.preprints.2033v1 | CC-BY 4.0 Open Access | rec: 9 May 2016, publ: 9 May 2016

(2791 ± 178.1 versus 1653 ± 160 mean ± SEM) (Fig 1G, 1H and 1I). After twelve days *in vitro*, ZIKV infected neurospheres were vanished from culture (Fig 1I). These results reveal a time-course of cell death in neurospheres exposed to ZIKV infection. Thus, we decided to explore the consequences of ZIKV infection prior to cell death, by analysing neurospheres three days after the infection.

ZIKV alters growth of human neurospheres and formation of neuronal cells

At this stage, both mock and ZIKV-infected conditions form neurospheres (Fig 2A and 2B); however, infected neurospheres were significantly smaller in comparison to mock neurospheres (Fig 2C). Quantification of DAPI staining showed that the reduction in size correlates with a small number of cell nuclei in ZIKV-exposed neurospheres (Fig 2D). To further characterize the identity of the cells depleted by ZIKV, neurospheres were immunostained for markers of neural progenitors and neuronal identity. ZIKV-infected neurospheres reduced Nestin (Supplementary Fig 2D-3I) and SOX2 progenitor markers (Fig 2F, 2I, 2H). There was decrease also on MAP2 (Supplementary Fig 2J-2M) and HuC/HuDU C/D neuronal markers in ZIKV-infected neurospheres compared to mock-infected neurospheres (Fig 2E, 2I, 2L). This reduction in the number of neural progenitors and young neurons could be due to alterations in cell cycle. Flow cytometry analyses revealed that cells in ZIKV-infected neurospheres abnormally accumulate in a sub-G1 phase (Fig 2M and 2N). Together, these results suggest that ZIKV impairs the ability of neural progenitors to progress in the cell cycle and to differentiate into neurons.

PeerJ Preprints | https://doi.org/10.7287/peerj.preprints.2033v1 | CC-BY 4.0 Open Access | rec: 9 May 2016, publ: 9 May 2016

Quantitative shotgun proteomics and RNA-seq identify the fingerprint of ZIKV-infected neurospheres

To determine the molecular consequences of ZIKV infection, proteins and mRNA from ZIKV-and mock-infected neurospheres were extracted after 3 days *in vitro* and submitted to state-of-the-art quantitative label-free shotgun proteomics and extracted mRNA to unbiased RNA-seq analysis. Comparing the expression of the most differentially regulated proteins ($p<0.05$) in ZIKV-infected neurospheres versus mock-infected neurospheres, we detected 199 downregulated and 259 upregulated amongst them. Regarding RNA-seq, 26 downregulated and 64 upregulated genes were identified. As expected, many proteins involved in viral recognition were deregulated including TLR4 (toll-like receptor 4) and the RNA helicase DDX6 (Supplementary Fig 3).

Representation of gene ontology groups highlights the most relevant biological processes (Figure 3A and 3B), in which translation and cell cycle were the prominent ones (Figure 3A). Translational mechanisms of host cell are modulated by viral infection (Huys et al., 2013; Modhiran et al., 2015; Ward et al., 2011). Accordingly, ZIKV-infected neurospheres show downregulation of proteins related to cellular shutdown, such as organelle localization, regulation and protein folding (Figure 3B).

The arrest of cell cycle after ZIKV infection was previously described (Tang et al., 2016). To get further insight into the molecular pathways, we have performed a

PeerJ Preprints | https://doi.org/10.7287/peerj.preprints.2033v1 | CC-BY 4.0 Open Access | rec: 9 May 2016, publ: 9 May 2016

regulation analysis, integrating RNA-Seq information and predicting missing links to those altered pathways. The interactome of ZIKV-infected neurospheres deregulated proteins and genes (Figure 3C) predict cell cycle arrest and chromosomal instability. Our results suggest that this might occur due to downregulation of Cyclin E (CCNE2) (Figure 3C), in addition to upregulation of Cyclin-dependent kinase inhibitor 1A (*CDKN1A*), which prevents the activation of the Cyclin E/CDK2 complex, and functions as a regulator of cell cycle progression during G1. Although CDK2 was not directly regulated in the proteome and transcriptome analyses, causal network using Ingenuity pathway analysis (Ingenuity® Systems, www.ingenuity.com) predicted inhibition of CDK2. Top upstream predicted regulators, EIF4 (p-value $6.86x10^{-7}$) and TP53 (p-value $1.20x10^{-6}$), are both linked to cell cycle and translation. Interestingly, we found BRCA1 (breast cancer type 1 susceptibility protein) and MRE11A (double-strand break repair protein) directly connected to those regulators. Both BRCA1 and MRE11A are related to DNA damage signalling or cell elimination if DNA is not repaired. In agreement, analysis of cell cycle showed that ZIKV-infected neurospheres presented a pre-G1 enriched population, which is known to contain cells with damaged DNA (Kajstura et al., 2007) (Fig 2M-2N). Similarly, the observation of pyknotic nuclei suggests increased DNA damage in ZIKV-infected neurospheres (Supplementary Fig 2). Taken together, these results argue that ZIKV infection trigger the DNA repair machinery in neural stem cells.

In accordance to the cell cycle arrest, the neurogenic program was downregulated

PeerJ Preprints | https://doi.org/10.7287/peerj.preprints.2033v1 | CC-BY 4.0 Open Access | rec: 9 May 2016, publ: 9 May 2016

as observed by a decrease in the expression of the neurogenic differentiation 1 gene (*NEUROD1*) and Special AT-rich sequence-binding protein 2 (SATB2).

Altogether, these results suggest that ZIKV depletes the pool of neural progenitors, reduces neuronal production through upregulation of a network of viral translation and DNA repair machinery as well as downregulation of molecules associated with cell cycle and neuronal differentiation.

Discussion

Since 2015, ZIKV has been associated with primary microcephaly (Calvet et al., 2016; Mlakar et al., 2016). In order to gain insights into the molecular mechanisms of how ZIKV generates brain abnormalities, we applied proteomics and transcriptomics to identify the molecular fingerprint of human neural cells infected by the ZIKV variant circulating in Brazil.

In agreement with previous studies describing the effect of the African strain MR 766 in neural stem cells and brain organoids (Tang et al., 2016; Garcez et al., 2016; Qian et al., 2016), we demonstrate that ZIKV strain isolated in Brazil infects neurospheres, triggers caspase-mediated cell death in neural progenitors and reduces neuronal production. As a consequence, growth was reduced (Fig 1 and Fig 2).

Some of the deregulated genes after ZIKV infection had been previously described by the transcriptome analysis of MR 766 ZIKV-infected human neural progenitors

PeerJ Preprints | https://doi.org/10.7287/peerj.preprints.2033v1 | CC-BY 4.0 Open Access | rec: 9 May 2016, publ: 9 May 2016

(Tang et al., 2016). For instance, *CDKN1A* gene, a cyclin-dependent kinase inhibitor 1A, related to cell cycle arrest by preventing phosphorylation of cyclin-dependent kinases, was also found upregulated after MR 766 ZIKV infection (Tang et al., 2016). Other examples include the upregulation of *SESN2* and *GDF15*, involved in the response to cellular stress after injury (Lee et al., 2012; Tiwari et al., 2015) and downregulation of *ARNT2*, a bHLH factor required for neuronal differentiation (Hao et al., 2013).

On the other hand, our proteomics' results showed many other cellular pathways modulated by ZIKV in human neurospheres. Many RNA viruses hijack cellular proteins, particularly RNA binding proteins to support virus replication. ZIKV increased DDX6 expression and translation. DDX6 (also known as RCK/p54) is an ATP-dependent RNA helicase engaged in RNA processing bodies, which participate in translational suppression, mRNA degradation and miRNA biogenesis. Interestingly, upregulation of DDX6 was also observed after the exposure to other flaviviruses. Dengue virus (DENV), West Nile virus (WNV) and Hepatitis C virus (HCV) depend on DDX6 binding to double strand structures in 3'UTR region, which promotes virus RNA translation (Ariumi et al., 2011; Huys et al., 2013; Jangra et al., 2010; Ward et al., 2011). Furthermore, ZIKV infection modulates cellular proteins involved in the innate immune response to eliminate virus infection. Flavivirus RNA may be sensed by RIG-I-like receptors (RLR) or toll-like receptors members (TLR), depending on RNA structure and cellular location. ZIKV in neurospheres upregulated the levels of TLR4, a major receptor in virus-mediated innate immune

PeerJ Preprints | https://doi.org/10.7287/peerj.preprints.2033v1 | CC-BY 4.0 Open Access | rec: 9 May 2016, publ: 9 May 2016

response in neuronal cells against other flaviviruses, including WNV and Japanese Encephalitis virus (JEV) (Han et al., 2014; Szretter et al., 2009). Recently, it has been reported that ZIKV infection induces TLR3 in human skin fibroblast (Hamel et al., 2015), human brain organoids and mouse neurospheres (Dang et al., 2016). While TLR3 recognize viral double-stranded RNA, TLR4 is able to recognize viral envelope glycoproteins (Barton, 2007). Despite the fact that TLR3 and TLR4 present distinct mechanisms of viral recognition, both receptors share similar downstream pathways leading to proinflammatory cytokine production (Ahmed, 2013). This suggests that modulation of the innate immune response should be considered in the search for therapeutic interventions against ZIKV. Altogether, these data show that ZIKV infection modulate proteins involved in pathways such as: RNA processing bodies, miRNA biogenesis, translational initiation regulators, ribosomal proteins, innate immune response and neuronal development.

The effect of ZIKV infection during neurogenesis likely explains the consequences of the so-called congenital syndrome of ZIKV for brain formation. Our work provides insights into the molecular mechanisms of ZIKV infection on progenitor proliferation, differentiation and survival, thus improving our understanding of human brain malformations. Yet, further *in vivo* and epidemiological studies are needed in order to better understand how ZIKV is linked to malformations of the central nervous system.

PeerJ Preprints | https://doi.org/10.7287/peerj.preprints.2033v1 | CC-BY 4.0 Open Access | rec: 9 May 2016, publ: 9 May 2016

PeerJ Preprints NOT PEER-REVIEWED

Experimental procedures

All protocols and procedures were approved by the institutional research ethics committee of Hospital Copa D'Or (CEPCOPADOR) under approved protocol # 727.269.

Human induced pluripotent stem cells

Human induced pluripotent stem cells were cultured either with Essential 8 medium (Thermo Fisher Scientific, USA) containing DMEM/F12 and supplement, or mTeSR1 (Stemcell Technologies, USA) on Matrigel (BD Biosciences, USA) coated dishes. The colonies were chemically passaged (0.5 mM EDTA, Thermo Fisher Scientific, USA) every 5-7 days until they reached 70-80% confluence and maintained at 37°C in humidified air with 5% CO_2.

Human neural stem cells

Human induced pluripotent stem cells were cultured either with Essential 8 medium (Thermo Fisher Scientific, USA) containing DMEM/F12 and supplement, or mTeSR1 (Stemcell Technologies, USA), on Matrigel (BD Biosciences, USA) coated surface. The colonies were manually passaged every 5-7 days until they reached 70-80% confluence and maintained at 37°C in humidified air with 5% CO_2. To induce differentiation to Neural stem cells, Human iPS cells were split and 24 hours later medium was switched to PSC neural Induction Medium (Thermo Fisher Scientific, USA), containing Neurobasal medium and PSC supplement, according to

PeerJ Preprints | https://doi.org/10.7287/peerj.preprints.2033v1 | CC-BY 4.0 Open Access | rec: 9 May 2016, publ: 9 May 2016

manufacturer's protocol. Medium was changed every other day until day 7, when neural stem cells are split and expanded on neural induction medium (Advanced DMEM/F12 and Neurobasal medium (1:1) with neural induction supplement; Thermo Fisher Scientific, USA).

Human neurospheres

Neural stem cells were cultured until 80% confluence and split with Accutase (Merck-Millipore, Germany). Cells were resuspended in neural medium with half DMEM/F12 and half Neurobasal medium supplemented with 1X N2 and 1X B27 supplements. The suspended neural stem cells were grown under rotation at 90 rpm, and medium was replaced every 4 days. Pictures were acquired using with EVOS Cell Imaging System (Thermo Fisher Scientific, USA). Neurospheres area was measured with ImageJ (μm^2).

Infection of neural stem cells with ZIKV

ZIKV was isolated from the blood of a patient from Espírito Santo, Brazil. The virus was propagated in Vero cells. Neural stem cells were either mock or ZIKV-infected. At 96 hours post-infection (hpi), cytopathic effect was observed and conditioned media from mock and ZIKV-infected cells were harvested, centrifuged at 300 x g and stored at -80^{o}C. ZIKV genome was sequenced and strain identity was confirmed

PeerJ Preprints | https://doi.org/10.7287/peerj.preprints.2033v1 | CC-BY 4.0 Open Access | rec: 9 May 2016, publ: 9 May 2016

(accession number NC_012532). ZIKV titers were determined by plaque assay performed in Vero cells. Neural stem cells were ZIKV-infected at MOIs ranging MOI ranging from 0.25 to 0.0025. Cells were incubated with virus or mock for 2 hours, when medium containing virus particles was replaced with fresh medium.

RNA extraction and RT-PCR

ZIKV stock sample was analyzed by RT-PCR to detect Zika, chikungunya and dengue viruses. Briefly, viral RNA was extracted using QIAamp MinElute Virus Spin Kit (Qiagen, Netherlands) and cDNA synthesis was performed with High-Capacity cDNA Reverse Transcription Kit (Thermo Fisher Scientific, USA) according to the manufacturer's instructions. RT-PCR was performed using using TaqMan Universal Master Mix (Thermo Fisher Scientific, USA) on 7500 Real-Time PCR System (Applied Biosystems) with primers and probes specifically designed for ZIKV (Lanciotti et al., 2008), CHIKV (Lanciotti, 2007) and DENV (Menting et al., 2011).

Immunostaining

Neurospheres were fixed with 4% paraformaldehyde (Sigma-Aldrich, USA) in phosphate-buffered saline for 15 min at 37□, cryoprotected in sucrose solution, mounted in OCT embedding compound and frozen at -20□. Thin sections (20 µm) were obtained with cryostat (Leica, Germany), permeabilized with 0.3% Triton X-100 (Sigma-Aldrich, USA), incubated in 50 mM ammonium chloride, followed by blocking with 3% bovine serum albumin (Sigma-Aldrich, USA) and overnight

PeerJ Preprints | https://doi.org/10.7287/peerj.preprints.2033v1 | CC-BY 4.0 Open Access | rec: 9 May 2016, publ: 9 May 2016

incubation with rabbit anti-human-Sox2 (1:100; Merck-Millipore, Germany), rabbit anti-human-caspase 3 active (cleaved) form (1:100; Merck-Millipore, Germany), mouse anti-human-HuC/HuD neuronal protein (16A11) (1:100, Invitrogen, EUA) and mouse anti-flavivirus group antigen antibody (clone 4G2, 1:100). Subsequently, samples were incubated with secondary antibodies: goat anti-rabbit Alexa Fluor 488 IgG (1:400; Thermo Fisher Scientific, USA) and goat anti-mouse Alexa Fluor 594 IgG (1:400; Thermo Fisher Scientific, USA). Nuclei were stained with 0.5 µg/mL 4′-6-diamino-2-phenylindole (DAPI) for 5 min. Images of three neurosphere slices of each condition were acquired with TCS SP8 confocal microscope (Leica, Germany) with an oil immersion 20x objective, high numerical apertures (NA). Total number of cells was calculated by DAPI stained nuclei. Image analysis was performed by applying segmentation algorithms for each channel using image analysis software Columbus (PerkinElmer, USA). Briefly, neurosphere slices total area was measured and elements inside that area were counted or measured. The ratio between the number of elements or the area occupied by a specific staining was calculated for each specific slice and results are represented as average of three slices for each condition.

Cresyl Violet staining and pyknotic nuclei analyses

Neurospheres were cut and stained with cresyl violet. Photomicrographs were taken with a magnification of 400X in an Axioplan Zeiss microscope. Cells displaying condensed pyknotic and fragmented nuclei were identified, counted under ImageJ

PeerJ Preprints | https://doi.org/10.7287/peerj.preprints.2033v1 | CC-BY 4.0 Open Access | rec: 9 May 2016, publ: 9 May 2016

2.0 (NIH) and grouped in the category “pyknotic nuclei”. Percentage of pyknotic nuclei was determined after normalization against total cell number.

Quantitative Proteomics and Data Processing Analyses

Qualitative and quantitative proteomic analyses were performed in a bidimensional micro UPLC tandem nanoESI-UDMSE platform by multiplexed data-independent acquisitions (DIA) experiments (Distler et al. 2014). 2D-RP/RP Acquity UPLC M-Class System (Waters Corporation, USA) coupled to a Synapt G2-Si mass spectrometer (Waters Corporation, USA) was used.

Peptide loads were carried to separation in a nanoACQUITY UPLC HSS T3 Column (1.8 µm, 75 µm X 150mm; Waters Corporation, USA). Peptide elutions were achieved by using an acetonitrile gradient from 7% to 40% (v/v) for 95 min at a flow rate of 0.4 µL /min directly into a Synapt G2-Si. For every measurement, the mass spectrometer was operated in resolution mode with an m/z resolving power of about 40 000 FWHM, using ion mobility with a cross-section resolving power at least 40 Ω /ΔΩ. MS/MS analyses were performed by nano-electrospray ionization in positive ion mode nanoESI (+) and a NanoLock Spray (Waters, UK) ionization source. The lock mass channel was sampled every 30 sec. The mass spectrometer was calibrated with an MS/MS spectrum of [Glu1]-Fibrinopeptide B human (Glu-Fib) solution that was delivered through the reference sprayer of the NanoLock Spray source.

PeerJ Preprints | https://doi.org/10.7287/peerj.preprints.2033v1 | CC-BY 4.0 Open Access | rec: 9 May 2016, publ: 9 May 2016

Proteins were identified and quantitative data were processed by using dedicated algorithms and cross-matched with the Uniprot human proteome database, version 2015/11 (70,225 entries), with the default parameters for ion accounting and quantitation (Li et al 2009). The databases used were reversed "on the fly" during the database queries and appended to the original database to assess the false-positive identification rate. For proper spectra processing and database searching conditions, we used Progenesis QI for proteomics software package with Apex3D, peptide 3D, and ion accounting informatics (Waters). This software starts with LC-MS data loading, then performs alignment and peak detection, which creates a list of interesting peptide ions (peptides) that are explored within Peptide Ion Stats by multivariate statistical methods; the final step is protein identity. The following parameters were considered in identifying peptides: 1) Digestion by trypsin allowing one missed cleavage; 2) methionine oxidation was considered a variable modification and carbamidomethylation (C), fixed modification; 3) false discovery rate (FDR) less than 1%. Identifications that did not satisfy these criteria were rejected.

Pathway and functional correlation analysis

Differentially expressed genes and proteins were analysed. Functional annotation analysis tool DAVID v 6.7 (http://niaid.abcc.ncifcrf.gov) was used to identify over-represented ontological groups amongst differentially expressed proteins of mock

PeerJ Preprints | https://doi.org/10.7287/peerj.preprints.2033v1 | CC-BY 4.0 Open Access | rec: 9 May 2016, publ: 9 May 2016

and ZIKV-infected neurospheres and to group proteins into functional categories (Huang et al., 2009a, 2009b). Whole genome was used as a background list. The over-represented GO terms (GOTERM_ALL level) using default settings and $p \leq 0.01$ under Fisher exact test. Ingenuity® Pathway Analysis (IPA®, QIAGEN Redwood City, USA, www.qiagen.com/ingenuity), was used to identify proteins and genes that may be part of pathway dysregulation caused by ZIKV. IPA® core analysis was performed using experimentally observed data, with canonical pathways, diseases and biological functions, and networks explored in detail. The refinement of the network generated by IPA® was performed applying the following parameters: direct/indirect interactions, experimentally observed as confidence level, human as species. In addition, we explored the protein-protein and gene-protein interactome using most relevant biological functions, as an interactive representation that shows the molecular relationship between molecules from the dataset based on Ingenuity Knowledge Database. In addition, protein-protein regulatory network information from high confidence STRING interactions (www.string-db.org) was added to this interactome (Jensen et al., 2009).

RNA-seq

Total RNA isolation from both conditions of neurospheres samples (MOCK and ZIKV infection) was done with *iPrep PureLink Total RNA Kit* (Thermo Fisher Scientific, USA). For total RNA quantitation and quality analyses we used *Qubit RNA HS Assay Kit* (Thermo Fisher Scientific, USA) and *Agilent RNA 6000 Pico Kit* (Agilent

PeerJ Preprints | https://doi.org/10.7287/peerj.preprints.2033v1 | CC-BY 4.0 Open Access | rec: 9 May 2016, publ: 9 May 2016

Technologies, USA). RNA-seq was performed using duplicated samples for each condition, libraries were built using *TruSeq Stranded mRNA Library Prep Kits* (Illumina, USA) according manufacturer's instructions. To evaluate fragment average and quantify libraries we used Agilent *2100 BioAnalyzer and High Sensitivity DNA Kit (*Agilent Technologies, USA) and a *qPCR-based KAPA library quantification kit* (KAPA Biosystems, USA), finally we pooled libraries with 20 pM of final concentration to following sequencing steps. For paired-end sequencing we used *MiSeq Sequencing System* (Illumina, USA) platform and *MiSeq Reagent Kit v3 (150 cycles).*

Illumina reads underwent quality control analysis using FastQC (http://www.bioinformatics.babraham.ac.uk/projects/fastqc/). The reads were aligned with TopHat version 2.1.1 (Kim et al., 2013) using the EMBL human genome GRCh37 as reference. Aligned reads were assembled *de novo* using CuffLinks version 2.2.1 (Trapnell et al., 2010). FPKM (Fragments Per Kilobase of transcript per Million reads mapped) values, which reflect mRNA expression levels, were generated using CuffDiff that is part of CuffLinks software. The R (Trapnell, 2012) package CummeRbund (R Core Team, 2012) was used to visualize the results. Ingenuity Pathway Analysis (www.ingenuity.com; Ingenuity Systems, Redwood City, CA, USA) was employed to identify biological functions associated with the differentially expressed genes.

PeerJ Preprints | https://doi.org/10.7287/peerj.preprints.2033v1 | CC-BY 4.0 Open Access | rec: 9 May 2016, publ: 9 May 2016

Viral RNA isolation and genome sequencing

First, viral RNA was isolated from infected neurospheres using iPrep PureLink Virus Kit (Thermo Fisher Scientific) and the cDNA synthesis reaction was performed using cDNA Synthesis System Kit (Roche), with random primers. After, PCR was done using specific primers to Asian ZIKV genotype sequence to get amplicons for sequencing. Amplicons were fragmented by enzymatic digestion and libraries built by the automated AB Library Builder System (Applied Biosystems). Libraries were submitted to emulsion PCR using the automated Ion OneTouch 2 platform. The emulsion PCR reaction was loaded on a 318v2 chip and the sequencing reaction was performed on the Ion PGM™ (Thermo Fisher Scientific, USA).

Genome assembly and phylogenetic analysis

Genome assembly was performed using Geneious v.9.1.3 using the genome of a Zika virus strain isolated in Brazil as reference (accession number KU926310). Minimum overlap and minimum overlap Identity parameter values were 40 and 95%, respectively. We obtained a partial sequence including partial envelope, NS1, NS2A, NS2B and NS3 from ZIKV genome. The obtained genome from BR_ZIKV_AB_ES isolate was deposited in GenBank with accession number KX212103.

The genomic sequence of BR_ZIKV_AB_ES was aligned with other ZIKV sequences available in NCBI using Mafft v.7 (Katoh and Standley, 2013). Measurement of

PeerJ Preprints | https://doi.org/10.7287/peerj.preprints.2033v1 | CC-BY 4.0 Open Access | rec: 9 May 2016, publ: 9 May 2016

phylogenetic signal in the aligned dataset was done using likelihood mapping test, as employed in Tree-Puzzle v 5.2 (Schmidt et al., 2002). The analysis revealed only 17% unresolved and 2.8 % partly resolved quartets, indicating that the dataset has a strong phylogenetic signal. The set of aligned data was submitted to jModelTest v.1.2.7 (Darriba et al., 2012), in order to find the best nucleotide substitution model. The construction of the phylogenetic tree was performed with maximum likelihood (ML) method (Myung, 2003) using RaxML v.8.0 (Stamatakis, 2014). A bootstrap test with 1,000 replicates was applied to provide confidence values (Felsenstein, 1985) (Supplementary Fig 1A). Genetic distances amongst strains were calculated using MEGA 6.06 (Tamura et al., 2013).

Author contributions:

P.P.G. and S.K.R. conceived all experiments and wrote the manuscript. J.M.N., J.S.C. and D.M.S. acquired, analysed and interpreted the proteome and molecular fingerprint data; J.V, H.F and J.V. acquired, analysed and interpreted transcriptome and molecular fingerprint data; J.M.N. analysed the combined proteome and transcriptome interactions. R.M.C acquired, quantified neurospheres immunohistochemistry and prepared manuscript figures; R.D. performed cell cycle and qPCR experiments; P.T. quantified pyknotic cells; L.M.H. amplified and titrated ZIKV; E.C.L. and G.V performed immunohistochemistry, cultivated neural stem cells; J.S. derived the iPS cells; P.S. and A.B.P isolated ZIKV; R.S.A. and A.T. provided the

PeerJ Preprints | https://doi.org/10.7287/peerj.preprints.2033v1 | CC-BY 4.0 Open Access | rec: 9 May 2016, publ: 9 May 2016

laboratory structure and viral reagents. All authors discussed the results and contributed intellectually on the manuscript.

Acknowledgments:

The authors thank the excellent technical support of Ismael Gomes, Dr. Renata Maciel for providing neural stem cells and Dr. Sandro Patroca da Silva for the phylogenetic and bioinformatic helpful advises. Authors also thank Fabricio Pamplona and Mind the Graph. Funds (not specifically for Zika virus studies) were provided by the Brazilian Development Bank (BNDES); Funding Authority for Studies and Projects (FINEP); National Council of Scientific and Technological Development (CNPq); Foundation for Research Support in the State of Rio de Janeiro (FAPERJ); the São Paulo Research Foundation (FAPESP, grants 14/21035-0, 14/14881-1, 13/08711-3 and 14/10068-4); and fellowships from the Coordination for the Improvement of Higher Education Personnel (CAPES).

References

Ahmed, S., Maratha, A., Butt, A.Q., Shevlin, E. and Miggin, S.M. (2013). TRIF-mediated TLR3 and TLR4 signaling is negatively regulated by ADAM15. J. Immunol. 190, 2217–28.

PeerJ Preprints | https://doi.org/10.7287/peerj.preprints.2033v1 | CC-BY 4.0 Open Access | rec: 9 May 2016, publ: 9 May 2016

Ariumi, Y., Kuroki, M., Kushima, Y., Osugi, K., Hijikata, M., Maki, M., Ikeda, M. and Kato, N. (2011). Hepatitis C virus hijacks P-body and stress granule components around lipid droplets. J. Virol. 85, 6882–92.

Barton, G.M. (2007). Viral recognition by Toll-like receptors. Semin. Immunol. 19, 33–40. doi:10.1016/j.smim.2007.01.003

Calvet, G., Aguiar, R.S., Melo, A.S.O., Sampaio, S.A., de Filippis, I., Fabri, A., Araujo, E.S.M., de Sequeira, P.C., de Mendonça, M.C.L., de Oliveira, L., Tschoeke, D.A., Schrago, C.G., Thompson, F.L., Brasil, P., dos Santos, F.B., Nogueira, R.M.R., Tanuri, A. and de Filippis, A.M.B. (2016). Detection and sequencing of Zika virus from amniotic fluid of fetuses with microcephaly in Brazil: a case study. Lancet Infect. Dis. 1–8.

Dang, J., Tiwari, S.K., Lichinchi, G., Qin, Y., Lichinchi, G., Patil, V.S., Eroshkin, A.M. and Rana, T.M. (2016). Zika Virus Depletes Neural Progenitors in Human Cerebral Organoids through Activation of the Innate Short Article Zika Virus Depletes Neural Progenitors in Human Cerebral Organoids through Activation of the Innate Immune Receptor TLR3. Cell Stem Cell . doi:10.1016/j.stem.2016.04.014

PeerJ Preprints | https://doi.org/10.7287/peerj.preprints.2033v1 | CC-BY 4.0 Open Access | rec: 9 May 2016, publ: 9 May 2016

Darriba, D., Taboada, G.L., Doallo, R. and Posada, D. (2012). jModelTest 2: more models, new heuristics and parallel computing. Nat. Methods 9, 772.

Felsenstein, J. (1985). Confidence Limits on Phylogenies: An Approach Using the Bootstrap. Evolution (N. Y). 39, 783.

Garcez, P.P., Loiola, E.C., Madeiro da Costa, R., Higa, L.M., Trindade, P., Delvecchio, R., Nascimento, J.M., Brindeiro, R., Tanuri, A. and Rehen, S.K. (2016). Zika virus impairs growth in human neurospheres and brain organoids. Science. doi:10.1126/science.aaf6116

Gilmore, E.C. and Walsh, C.A. (2013). Genetic causes of microcephaly and lessons for neuronal development. Wiley Interdiscip. Rev. Dev. Biol. 2, 461–78.

Hamel, R., Dejarnac, O., Wichit, S., Ekchariyawat, P., Neyret, A., Luplertlop, N., Perera-Lecoin, M., Surasombatpattana, P., Talignani, L., Thomas, F., Cao-Lormeau, V.-M., Choumet, V., Briant, L., Desprès, P., Amara, A., Yssel, H. and Missé, D. (2015). Biology of Zika Virus Infection in Human Skin Cells. J. Virol. 89, 8880–96.

Han, Y.W., Choi, J.Y., Uyangaa, E., Kim, S.B., Kim, J.H., Kim, B.S., Kim, K. and Eo, S.K. (2014). Distinct dictation of Japanese encephalitis virus-induced

PeerJ Preprints | https://doi.org/10.7287/peerj.preprints.2033v1 | CC-BY 4.0 Open Access | rec: 9 May 2016, publ: 9 May 2016

neuroinflammation and lethality via triggering TLR3 and TLR4 signal pathways. PLoS Pathog. 10, e1004319.

Hao, N., Bhakti, V.L.D., Peet, D.J. and Whitelaw, M.L. (2013). Reciprocal regulation of the basic helix-loop-helix/Per-Arnt-Sim partner proteins, Arnt and Arnt2, during neuronal differentiation. Nucleic Acids Res. 41, 5626–38.

Huang, D.W., Sherman, B.T. and Lempicki, R.A. (2009a). Bioinformatics enrichment tools: paths toward the comprehensive functional analysis of large gene lists. Nucleic Acids Res. 37, 1–13.

Huang, D.W., Sherman, B.T. and Lempicki, R.A. (2009b). Systematic and integrative analysis of large gene lists using DAVID bioinformatics resources. Nat. Protoc. 4, 44–57.

Huys, A., Thibault, P.A. and Wilson, J.A. (2013). Modulation of hepatitis C virus RNA accumulation and translation by DDX6 and miR-122 are mediated by separate mechanisms. PLoS One 8, e67437.

Jangra, R.K., Yi, M. and Lemon, S.M. (2010). DDX6 (Rck/p54) is required for efficient hepatitis C virus replication but not for internal ribosome entry site-directed translation. J. Virol. 84, 6810–24.

PeerJ Preprints | https://doi.org/10.7287/peerj.preprints.2033v1 | CC-BY 4.0 Open Access | rec: 9 May 2016, publ: 9 May 2016

PeerJ Preprints NOT PEER-REVIEWED

Jensen, L.J., Kuhn, M., Stark, M., Chaffron, S., Creevey, C., Muller, J., Doerks, T., Julien, P., Roth, A., Simonovic, M., Bork, P. and von Mering, C. (2009). STRING 8--a global view on proteins and their functional interactions in 630 organisms. Nucleic Acids Res. 37, D412–6.

Kajstura, M., Halicka, H.D., Pryjma, J. and Darzynkiewicz, Z. (2007). Discontinuous fragmentation of nuclear DNA during apoptosis revealed by discrete "sub-G1" peaks on DNA content histograms. Cytometry. A 71, 125–31.

Katoh, K. and Standley, D.M. (2013). MAFFT multiple sequence alignment software version 7: improvements in performance and usability. Mol. Biol. Evol. 30, 772–80.

Kim, D., Pertea, G., Trapnell, C., Pimentel, H., Kelley, R. and Salzberg, S.L. (2013). TopHat2: accurate alignment of transcriptomes in the presence of insertions, deletions and gene fusions. Genome Biol. 14, R36.

Lanciotti, R.S., Kosoy, O.L., Laven, J.J., Panella, A.J., Velez, J.O., Lambert, A.J. and Campbell, G.L. (2007). Chikungunya virus in US travelers returning from India, 2006. Emerg. Infect. Dis. 13, 764–7.

PeerJ Preprints | https://doi.org/10.7287/peerj.preprints.2033v1 | CC-BY 4.0 Open Access | rec: 9 May 2016, publ: 9 May 2016

Lanciotti, R.S., Kosoy, O.L., Laven, J.J., Velez, J.O., Lambert, A.J., Johnson, A.J., Stanfield, S.M. and Duffy, M.R. (2008). Genetic and Serologic Properties of Zika Virus Associated with an Epidemic, Yap State, Micronesia, 2007. Emerg. Infect. Dis. 14, 1232–1239.

Lee, J.H., Budanov, A.V., Talukdar, S., Park, E.J., Park, H.L., Park, H.W., Bandyopadhyay, G., Li, N., Aghajan, M., Jang, I., Wolfe, A.M., Perkins, G.A., Ellisman, M.H., Bier, E., Scadeng, M., Foretz, M., Viollet, B., Olefsky, J. and Karin, M. (2012) Maintenance of metabolic homeostasis by Sestrin2 and Sestrin3. Cell Metab. 16, 311–21.

Li, C., Li, X., Miao, Y., Wang, Q., Jiang, W., Xu, C., Li, J., Han, J., Zhang, F., Gong, B. and Xu, L. (2009). SubpathwayMiner: a software package for flexible identification of pathways. Nucleic Acids Res. 37, e131.

Menting, S., Thai, K.T.D., Nga, T.T.T., Phuong, H.L., Klatser, P., Wolthers, K.C., Binh, T.Q., de Vries, P.J. and Beld, M. (2011). Internally controlled, generic real-time PCR for quantification and multiplex real-time PCR with serotype-specific probes for serotyping of dengue virus infections. Adv. Virol. 2011, 514681. doi:10.1155/2011/514681

PeerJ Preprints | https://doi.org/10.7287/peerj.preprints.2033v1 | CC-BY 4.0 Open Access | rec: 9 May 2016, publ: 9 May 2016

Mlakar, J., Korva, M., Tul, N., Popović, M., Poljšak-Prijatelj, M., Mraz, J., Kolenc, M., Resman Rus, K., Vesnaver Vipotnik, T., Fabjan Vodušek, V., Vizjak, A., Pižem, J., Petrovec, M. and Avšič Županc, T. (2016). Zika Virus Associated with Microcephaly. N. Engl. J. Med. 1–8.

Modhiran, N., Watterson, D., Muller, D.A., Panetta, A.K., Sester, D.P., Liu, L., Hume, D.A., Stacey, K.J. and Young, P.R. (2015). Dengue virus NS1 protein activates cells via Toll-like receptor 4 and disrupts endothelial cell monolayer integrity. Sci. Transl. Med. 7, 304ra142. doi:10.1126/scitranslmed.aaa3863

Myung, I.J., 2003. Tutorial on maximum likelihood estimation. J. Math. Psychol. 47, 90–100.

Qian, X., Nguyen, H.N., Song, M.M., Hadiono, C., Ogden, S.C., Hammack, C., Yao, B., Hamersky, G.R., Jacob, F., Zhong, C., Yoon, K.-J., Jeang, W., Lin, L., Li, Y., Thakor, J., Berg, D.A., Zhang, C., Kang, E., Chickering, M., Nauen, D., Ho, C.-Y., Wen, Z., Christian, K.M., Shi, P.-Y., Maher, B.J., Wu, H., Jin, P., Tang, H., Song, H. and Ming, G.-L. (2016). Brain-Region-Specific Organoids Using Mini-bioreactors for Modeling ZIKV Exposure. Cell. doi:10.1016/j.cell.2016.04.032

Schmidt, H.A., Strimmer, K., Vingron, M. and von Haeseler, A. (2002). TREE-PUZZLE: maximum likelihood phylogenetic analysis using quartets and parallel computing. Bioinformatics 18, 502–4.

PeerJ Preprints | https://doi.org/10.7287/peerj.preprints.2033v1 | CC-BY 4.0 Open Access | rec: 9 May 2016, publ: 9 May 2016

Stamatakis, A. (2014). RAxML version 8: a tool for phylogenetic analysis and post-analysis of large phylogenies. Bioinformatics 30, 1312–3.

Szretter, K.J., Samuel, M.A., Gilfillan, S., Fuchs, A., Colonna, M. and Diamond, M.S. (2009). The immune adaptor molecule SARM modulates tumor necrosis factor alpha production and microglia activation in the brainstem and restricts West Nile Virus pathogenesis. J. Virol. 83, 9329–38.

Tang, H., Hammack, C., Ogden, S.C., Wen, Z., Qian, X., Li, Y., Yao, B., Shin, J., Zhang, F., Lee, E.M., Christian, K.M., Didier, R.A., Jin, P., Song, H. and Ming, G.-L. (2016). Zika Virus Infects Human Cortical Neural Progenitors and Attenuates Their Growth. Cell Stem Cell 18, 1–4.

Trapnell, C., Roberts, A., Goff, L., Pertea, G., Kim, D., Kelley, D.R., Pimentel, H., Salzberg, S.L., Rinn, J.L. and Pachter, L. (2012). Differential gene and transcript expression analysis of RNA-seq experiments with TopHat and Cufflinks. Nat. Protoc. 7, 562–78.

Trapnell, C., Williams, B.A., Pertea, G., Mortazavi, A., Kwan, G., van Baren, M.J., Salzberg, S.L., Wold, B.J. and Pachter, L., (2010). Transcript assembly and

PeerJ Preprints | https://doi.org/10.7287/peerj.preprints.2033v1 | CC-BY 4.0 Open Access | rec: 9 May 2016, publ: 9 May 2016

quantification by RNA-Seq reveals unannotated transcripts and isoform switching during cell differentiation. Nat. Biotechnol. 28, 511–5.

Tiwari, K.K., Moorthy, B. and Lingappan, K. (2015). Role of GDF15 (growth and differentiation factor 15) in pulmonary oxygen toxicity. Toxicol. In Vitro 29, 1369–76.

Ward, A.M., Bidet, K., Yinglin, A., Ler, S.G., Hogue, K., Blackstock, W., Gunaratne, J. and Garcia-Blanco, M.A. (2011). Quantitative mass spectrometry of DENV-2 RNA-interacting proteins reveals that the DEAD-box RNA helicase DDX6 binds the DB1 and DB2 3' UTR structures. RNA Biol. 8, 1173–86.

Figure legends:

Figure 1: ZIKV triggers cell death in human neurospheres

(A-F) Immunocytochemistry for the flavivirus antigen (red) and cleaved caspase-3 (green) counterstained with DAPI (blue) on Mock- and ZIKV-infected neurospheres. (G) Quantification of flavivirus antigen and (H) cleaved caspase-3 fluorescence intensity. Individual sample data were normalized against the average of Mock-infected experimental group. (I-J)Brightfield photomicrographs of Mock- and ZIKV-infected neurospheres at day 12. Calibration Bar: 100µm. (K) Time-course of

PeerJ Preprints | https://doi.org/10.7287/peerj.preprints.2033v1 | CC-BY 4.0 Open Access | rec: 9 May 2016, publ: 9 May 2016

neurospheres viability of Mock- and ZIKV-infected experimental groups. Data presented as mean ± SD, n=4, Student's t-test, ** p<0.01.

Figure 2: ZIKV reduces the growth of neurospheres, by depleting the pool of neural progenitors and the generation of neurons

(A-B) Brightfield photomicrographs of Mock- and ZIKV-infected neurospheres. Calibration Bar: 100μm. Bar graphs showing a reduction of neurospheres area (C) and in numbers of nuclei per neurosphere area (D) on ZIKV-infected experimental group. (E-K) Immunocytochemistry for the neuronal marker HuC/D (red) and the neural progenitor marker SOX2 (green) counterstained with DAPI (blue). Quantification of HuC/D and SOX2 fluorescence intensity shows a decrease of both markers on ZIKV-infected neurospheres. (M-N) Flow cytometry distribution analyses of neurospheres at subG1 phase of cell cycle 3 days after ZIKV or mock infection. Differences on bar graphs were expressed by fold change in relation to the average values of the Mock-infected group. Data presented as mean ± SD, n=4, Student's t-test, * p<0.05; ** p<0.01; *** p<0.001.

Figure 3: ZIKV alters translation, causing arrest of the cell cycle and decreasing neural differentiation in human neurospheres

Functional enrichment of gene ontology biological functions of upregulated (A) and downregulated (B) proteins. (C) Network interactive representation of molecular relationship between regulated molecules on ZIKV-infected neurospheres,

PeerJ Preprints | https://doi.org/10.7287/peerj.preprints.2033v1 | CC-BY 4.0 Open Access | rec: 9 May 2016, publ: 9 May 2016

predicting downregulation of CDK2 and inhibition of cell cycle progress. Interactome analyzed from the dataset based on Ingenuity Knowledge Database (www.ingenuity.com) and String (string-db.org).

Supplemental Information:

Supplementary Figure 1: Asian genotype of ZIKV isolated in Brazil

(A) Phylogenetic analysis including BRZIKV_AB_ES isolate and ZIKV available sequences. Both genotypes are represented on this ML (*maximum likelihood*) tree: in blue, Asian, in green, African genotype and, highlighted in red, the partial ZIKV sequence obtained from infected neurospheres here described (BRZIKV_AB_ES). This analysis demonstrates that the isolated strain belongs to Asian genotype. The genetic distance of BRZIKV_AB_ES to strains isolated in Brazil (Asian) is only 0.2 % and to the MR strain 766 (African) is 11.6%. (B) ZIKV stock sample was analyzed by RT-PCR to detect Zika (blue lines), chikungunya (red line) and Dengue (black line) viruses

Supplementary Figure 2:

ZIKV infection increases the number of cells displaying pyknosis and decreases progenitors and neuronal markers on neurospheres

(A-B) Brightfield photomicrographs of cells displaying condensed pyknotic (arrows) and fragmented nuclei (arrowheads). Calibration Bar: 10µm.

PeerJ Preprints | https://doi.org/10.7287/peerj.preprints.2033v1 | CC-BY 4.0 Open Access | rec: 9 May 2016, publ: 9 May 2016

(C) Quantification of the percentage of pyknotic nuclei found on Mock- and ZIKV-infected neurospheres. Data presented as mean ± SEM, n=4, Student's t-test, ** $p<0.01$.

Immunocytochemistry for the progenitor marker nestin (red) on mock- (D-E) and on ZIKV-infected neurospheres (F-G) counterstained with DAPI (blue). (H) Quantification of neural progenitor marker nestin fluorescence intensity. Immunocytochemistry for the neuronal marker MAP2 (red) on mock- (I-J) and ZIKV-infected neurospheres (K-L) counterstained with DAPI (blue). (M) Quantification of neuronal marker MAP2 fluorescence intensity. Data presented as mean ± SD, n=4, Student's t-test, *$p < 0.05$. ; *** $p<0.001$ Calibration Bar: 100µm

Supplementary Figure 3:

ZIKV infection upregulates proteins required for viral replication.

Network interactive representation of molecular relationship between regulated molecules on ZIKV-infected neurospheres. Interactome analyzed from the dataset based on Ingenuity Knowledge Database (www.ingenuity.com) and String (string-db.org).

PeerJ Preprints | https://doi.org/10.7287/peerj.preprints.2033v1 | CC-BY 4.0 Open Access | rec: 9 May 2016, publ: 9 May 2016

PeerJ Preprints NOT PEER-REVIEWED

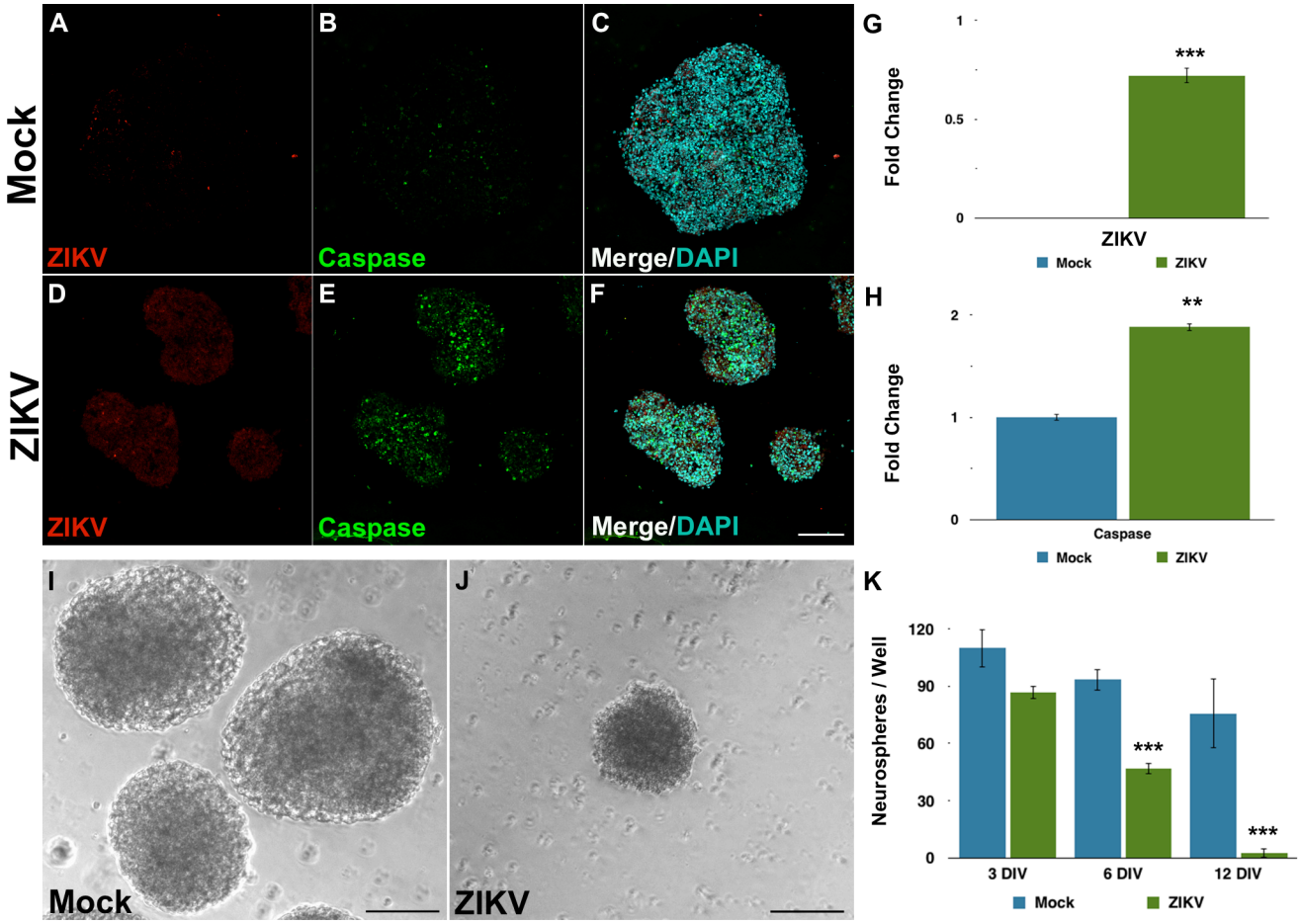

PeerJ Preprints | https://doi.org/10.7287/peerj.preprints.2033v1 | CC-BY 4.0 Open Access | rec: 9 May 2016, publ: 9 May 2016

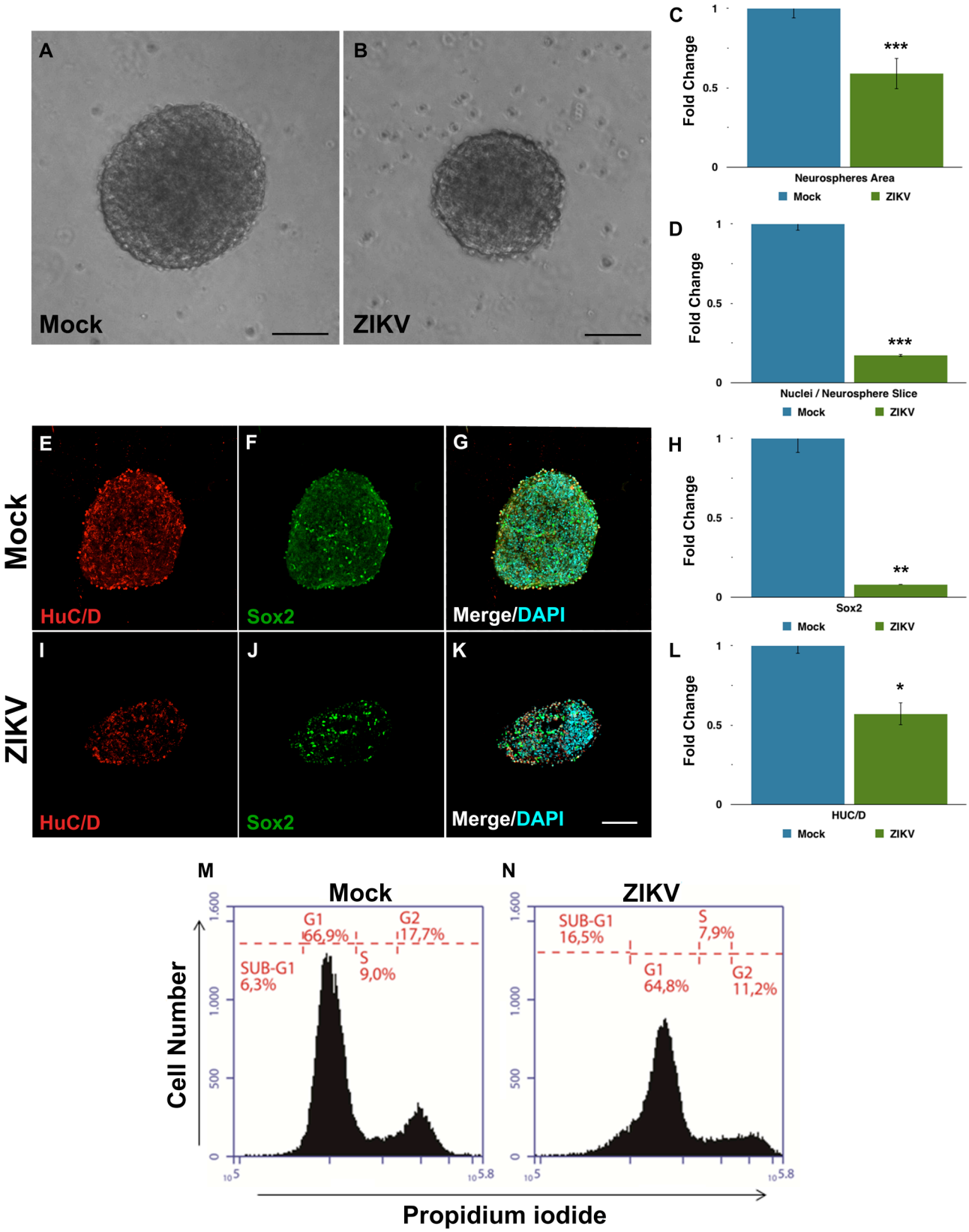
A
Mock
B
ZIKV
C
Fold Change
1
0.5
0
***
Neurospheres Area
Mock
ZIKV
D
Fold Change
1
0.5
0
***
Nuclei / Neurosphere Slice
Mock
ZIKV
Mock
E
HuC/D
F
Sox2
G
Merge/DAPI
ZIKV
I
HuC/D
J
Sox2
K
Merge/DAPI
H
Fold Change
1
0.5
0
**
Sox2
Mock
ZIKV
L
Fold Change
1
0.5
0
*
HUC/D
Mock
ZIKV
M
Mock
G1
66,9%
G2
17,7%
S
9,0%
SUB-G1
6,3%
N
ZIKV
SUB-G1
16,5%
S
7,9%
G1
64,8%
G2
11,2%
Cell Number
1.600
1.000
500
0
10^5
10^5.8
Propidium iodide

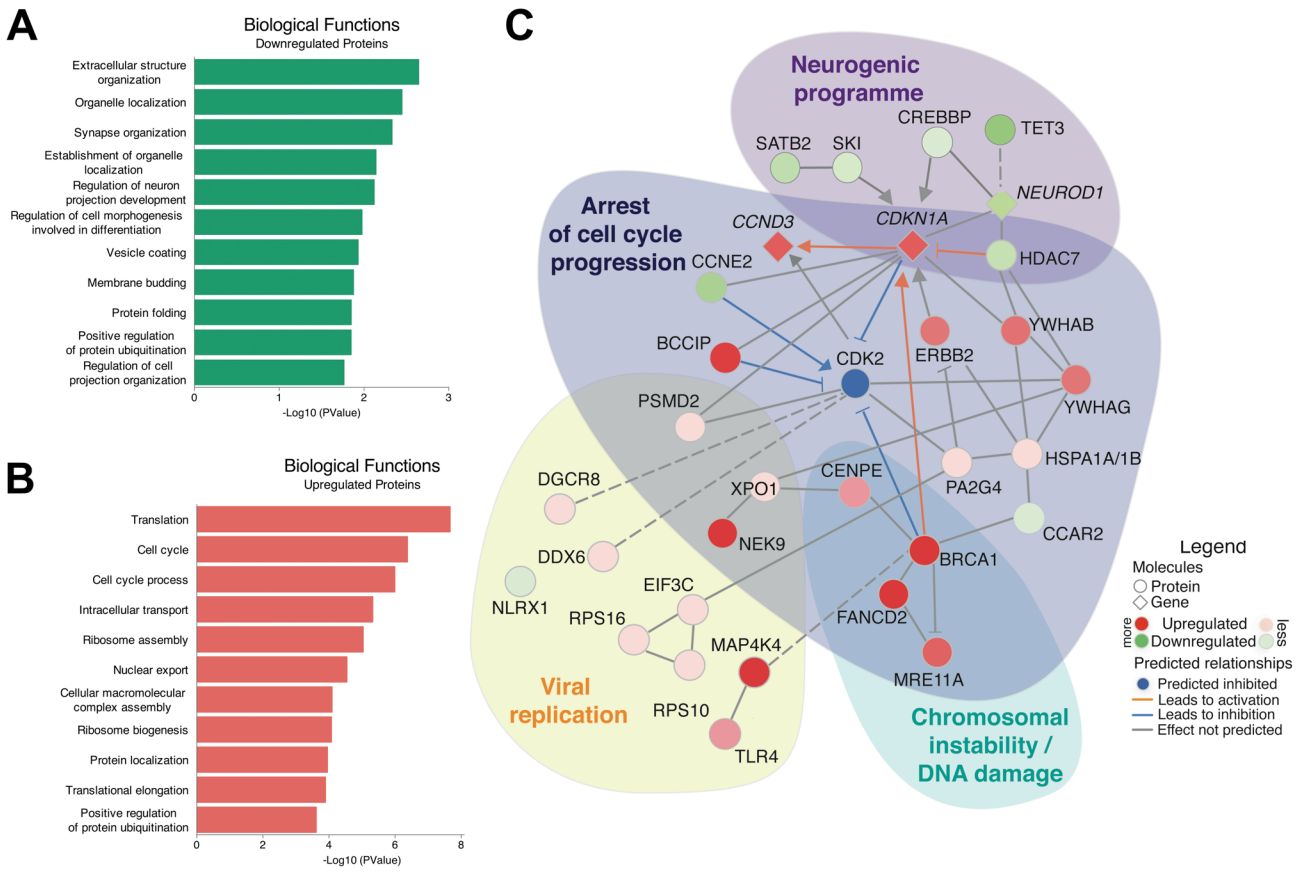
A
Biological Functions
Downregulated Proteins
Extracellular structure organization
Organelle localization
Synapse organization
Establishment of organelle localization
Regulation of neuron projection development
Regulation of cell morphogenesis involved in differentiation
Vesicle coating
Membrane budding
Protein folding
Positive regulation of protein ubiquitination
Regulation of cell projection organization
0
1
2
3
-Log10 (PValue)
B
Biological Functions
Upregulated Proteins
Translation
Cell cycle
Cell cycle process
Intracellular transport
Ribosome assembly
Nuclear export
Cellular macromolecular complex assembly
Ribosome biogenesis
Protein localization
Translational elongation
Positive regulation of protein ubiquitination
0
2
4
6
8
-Log10 (PValue)
C
Neurogenic programme
Arrest of cell cycle progression
Viral replication
Chromosomal instability / DNA damage
SATB2
SKI
CREBBP
TET3
NEUROD1
CCND3
CDKN1A
CCNE2
HDAC7
BCCIP
CDK2
ERBB2
YWHAB
PSMD2
YWHAG
HSPA1A/1B
DGCR8
XPO1
CENPE
PA2G4
CCAR2
NEK9
BRCA1
DDX6
NLRX1
EIF3C
RPS16
FANCD2
MAP4K4
MRE11A
RPS10
TLR4
Legend
Molecules
Protein
Gene
more
Upregulated
Downregulated
less
Predicted relationships
Predicted inhibited
Leads to activation
Leads to inhibition
Effect not predicted

PeerJ Preprints NOT PEER-REVIEWED

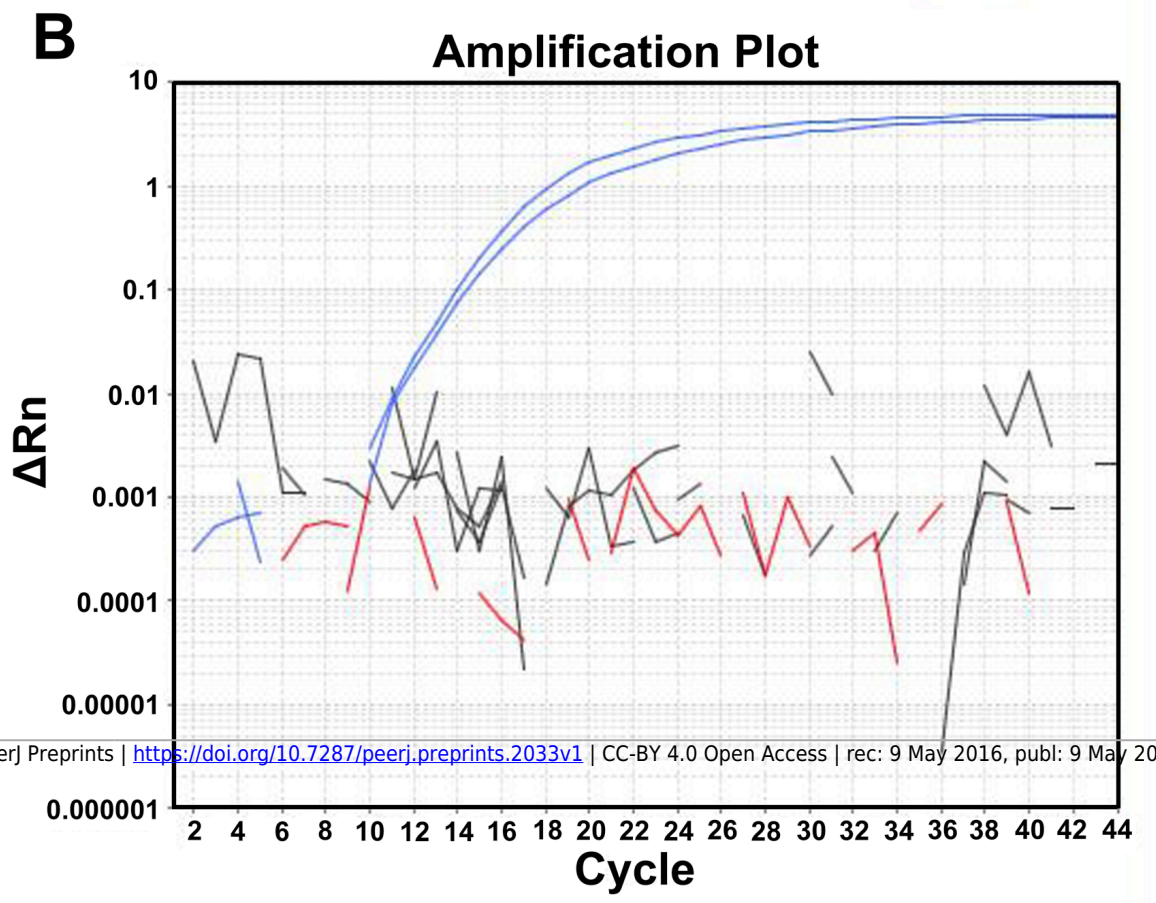

PeerJ Preprints | https://doi.org/10.7287/peerj.preprints.2033v1 | CC-BY 4.0 Open Access | rec: 9 May 2016, publ: 9 May 2016

PeerJ Preprints NOT PEER-REVIEWED

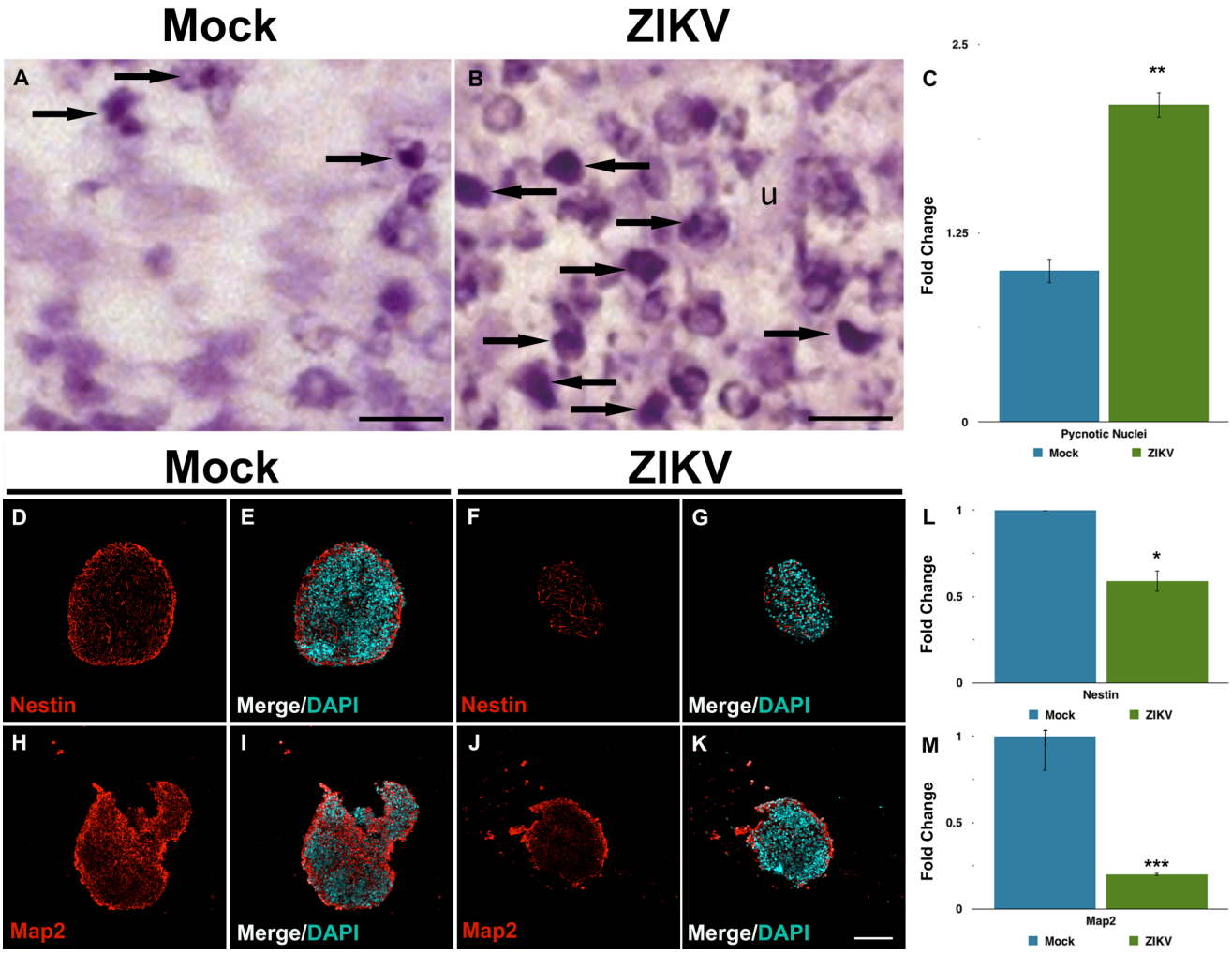

PeerJ Preprints NOT PEER-REVIEWED